

# Direct $\rho_L$ meson production in proton-proton and proton-antiproton collisions

C. Aydin<sup>1 \*</sup>, O. Uzun<sup>1 †</sup>, and A. I. Ahmadov<sup>2,3 ‡</sup>

<sup>1</sup> *Department of Physics, Karadeniz Technical University, 61080, Trabzon, Turkey*

<sup>2</sup> *Department of Theoretical Physics, Baku State University,*

*Z. Khalilov st. 23, AZ-1148, Baku, Azerbaijan*

<sup>3</sup>*Institute for Physical Problems, Baku State University,*

*Z. Khalilov st. 23, AZ-1148, Baku, Azerbaijan*

## Abstract

We have investigated the contribution of the Higher Twist (HT) Feynman diagrams to the large- $p_T$  inclusive  $\rho_L$  meson production cross section in proton-proton and proton-antiproton collisions and we discuss the phenomenological consequences of possible HT contributions to cross sections. To extract HT subprocesses from Leading Twist (LT) background, we use various  $\rho_L$  meson distribution amplitudes(DAs). In the numerical calculations, the dependencies of the HT contribution on the transverse momentum and the rapidity are discussed with special emphasis on DAs. Analysis of our results shows that HT contributions decrease more rapidly than LT contributions with increasing  $p_T$ . The preceding results demonstrate that HT contributions must be considered especially in the region of low  $p_T$  and the HT contribution to the cross-section depends on the choice of the meson distribution amplitudes.

PACS numbers: 12.38-t, 13.60.Le, 13.87.Ph, 14.40-n

Keywords: Higher-twist, Leading -twist,  $\rho$  meson distribution amplitudes

---

\* E-mail: coskun@ktu.edu.tr

† E-mail:oguzhan\_deu@hotmail.com

‡ E-mail: ahmadovazar@yahoo.com

## I. INTRODUCTION

Quantum chromodynamics (QCD) is the basic field theory of strong interactions used for describing hadronic processes. High- and low- energy dynamics of a hadronic process at large transverse momentum ( $p_T$ ) can be analyzed within the framework of the factorization theorem [1]. According to this theorem, high  $p_T$  hadronic processes can be separated into two parts each appearing at different energy scales. While the hard part that takes place between the interacting partons can be calculated by perturbative quantum chromodynamics (pQCD), the soft part that refers to the bound state dynamics of external hadrons is of nonperturbative nature. It has been observed that the high  $p_T$  hadronic processes such as the production of hadrons, prompt photons, and hadron jets are not described by the simple dependence predicted by the original parton model [2, 3].

The idea of direct hadron production was first considered in 1970s to explain the large fixed scalling exponents reported at ISR and fixed target FNAL energies [4]. Hadron production studies at large  $p_T$  provides a valuable testing ground for the perturbation regime of QCD and also information about both the parton distribution functions (PDFs) of hadrons and the parton to hadron fragmentation functions (FFs). Proton-proton collisions are known to be the most elementary interactions and form the very basic of our knowledge about the nature of high-energy particle collisions. For these reasons inclusive direct longitudinally polarized  $\rho_L$  meson production in  $pp$  proton-proton and  $p\bar{p}$  proton-antiproton collision processes has an important place in phenemologic research. Origin of the contributions to cross section to this processes can be separated into two parts

- Higher twist (HT) subprocesses  $q_1 + \bar{q}_2 \rightarrow \rho_L^+(\rho_L^-) + \gamma$  and,
- Leading twist (LT) subprocesses as the background of the HT subprocesses such as  $q + \bar{q} \rightarrow \gamma + g$ , where the gluon is fragmented to a  $\rho_L$  meson  $g \rightarrow \rho_L^+(\rho_L^-)$ , and  $q + g \rightarrow \gamma + q$ , where the quark is fragmented to a  $\rho_L$  meson  $q \rightarrow \rho_L^+(\rho_L^-)$ ,  $\bar{q} + g \rightarrow \gamma + \bar{q}$ , where the antiquark is fragmented to a  $\rho_L$  meson  $\bar{q} \rightarrow \rho_L^+(\rho_L^-)$  and so on.

LT is the standard processes of the pQCD, where hadrons are produced via fragmentation processes indirectly from the partons with the fractional momentum  $z$ . In contrast, HT processes are often understood as the direct hadron production, where the hadron is

produced directly in the hard subprocess without fragmentation [5]. A natural explanation for the large exponents observed in the hadron channel is the presence of important HT contributions from processes in which the detected hadron is produced directly in the hard subprocess due to the hadron distribution amplitude [6]. In a general QCD analysis of inclusive hadroproduction, all contributing leading and HT hard subprocesses should be considered [7]. In order to calculate LT contributions, parton interaction cross-sections and relevant distribution and FFs at the appropriate scales should be known. PDFs and FFs represent intrinsic constituents of the proton and the hadronization mechanism, respectively. These functions cannot be calculated using perturbation theory, therefore, they can be obtained from data for various types of hard-scattering processes. Due to the emergence of the hadron in the final state directly at the hard-scattering subprocess, calculation of HT contributions would require nonperturbative, processes-independent distribution amplitudes (DAs), instead of FFs.

DAs describing the distribution of partons inside the hadron, provides essential information on the nonperturbative structure of a hadron[8]. The choice of proper hadronic DA is one of the key components of analysis on the direct hadron production. During the past few decades, several important nonperturbative tools have been developed, which allow specific predictions for the hadronic DAs.

A main difficulty in making precise pQCD predictions is the uncertainty in determining the renormalization scale  $\mu_R$  of the running coupling  $\alpha_s(\mu_R^2)$  and also in factorization scale  $\mu_F$ . In the practical calculations, it is difficult to guess a simple physical scale of order of a typical momentum transfer in the process. In a common case, this problem for all orders is solved in Refs. [9] and [10]. In the present calculations for renormalization and factorization scales we used momentum squared carried by the hard gluon, which is obtained directly from Fig1.

Light vector and pseudoscalar meson production provides a reference for high-energy heavy-ion collisions. In fact, key information on the hot and dense state of strongly interacting matter produced in these collisions can be extracted measuring light meson [11]. Precision experimental studies of  $\rho_L$  meson production in proton-antiproton and proton-proton collisions at low energies are proposed in the experiment named PANDA [12]. The PANDA scientific program uses low-energy ranging between 1.5-15 GeV for interactions between protons and antiprotons, where this energy lies around the pion and  $\rho$  meson produc-

tion threshold. This program includes several measurements and it addresses fundamental questions of QCD by obtaining the detailed analyses of all possible mechanisms of meson pair production [13].

Many research papers can be found in the scientific literature on the contribution of the HT effects to the cross-section. Inclusive gluon production in pion-proton collisions [14], direct photon production in a pion-proton collision [15], pion production in proton-proton and photon-photon collisions [16–18] are some examples of these studies. Direct longitudinally polarized  $\rho_L$  meson production in the  $pp$  proton-proton and  $p\bar{p}$  proton-antiproton collision can be used to tune particle production models and they are the key probes of the hot and dense state of strongly interacting matter produced in heavy-ion collisions. Also, longitudinally polarized  $\rho_L$  meson production in the  $p\bar{p}$  collision is a very important task of the FAIR experiment.

In this study, we examine the contribution of the HT effects to inclusive  $\rho_L^\pm$  production at proton-antiproton and proton-proton collisions by using different  $\rho_L$  meson DAs which can be helpful for an explanation of the PENIUX and PANDA experiments. We have also given theoretical predictions of the inclusive  $\rho_L^\pm$  meson production in  $p\bar{p}$  and  $pp$  collisions by accounting for the leading order diagrams in partonic cross-sections.

We show that the HT terms contribute substantially to the inclusive meson cross-section at moderate transverse momenta. In addition, we demonstrate that HT reactions necessarily dominate in the kinematic limit where the transverse momentum approaches the phase-space boundary. Another important aspect of this study is the choice of the  $\rho_L$  meson DAs. In this respect, the HT Feynman diagrams have been computed by using various  $\rho_L$  meson DAs obtained by using light front quarks model, QCD sum rules and lattice QCD.

The rest of the paper is organized as follows: In Sec.II, formulas for LT cross-sections for  $\rho_L$  meson production are provided. In Sec. III, a brief information for the calculation of the HT contribution to cross-section and the formulas for the HT cross-section of the process  $pp \rightarrow \rho_L \gamma X$  and  $p\bar{p} \rightarrow \rho_L \gamma X$  are given. Numerical results for the cross-section and the discussion of the dependence on the cross-section on the  $\rho_L$  meson DA are provided in Sec. IV. Finally, the concluding remarks are stated in Sec. V.

## II. CONTRIBUTION OF THE LEADING TWIST DIAGRAMS

The LT subprocesses for the  $\rho_L$  meson production we take two subprocesses: (1) quark-antiquark annihilation  $q\bar{q} \rightarrow g\gamma$ , in which the  $\rho_L$  meson indirectly emitted from the gluon,  $g \rightarrow \rho_L^+(\rho_L^-)$  and (2) quark-gluon fusion,  $qg \rightarrow q\gamma$ , with subsequent fragmentation of final quark into a meson,  $q \rightarrow \rho_L^+(\rho_L^-)$ . The Mandelstam invariant variables for subprocesses  $q_1 + \bar{q}_2 \rightarrow \rho_L^+(\rho_L^-) + \gamma$  presented in Fig.1 are defined as

$$\hat{s} = -(p_1 + p_2)^2, \quad \hat{t} = -(p_1 - p_\rho)^2, \quad \hat{u} = -(p_1 - p_\gamma)^2. \quad (2.1)$$

In our calculations, the quarks masses are neglected. The corresponding cross- sections is obtained as

$$\frac{d\sigma}{d\hat{t}}(q\bar{q} \rightarrow g\gamma) = \frac{8}{9}\pi\alpha_E\alpha_s(Q^2)\frac{e_q^2}{\hat{s}^2}\left(\frac{\hat{t}}{\hat{u}} + \frac{\hat{u}}{\hat{t}}\right), \quad (2.2)$$

$$\frac{d\sigma}{d\hat{t}}(qg \rightarrow q\gamma) = -\frac{\pi e_q^2\alpha_E\alpha_s(Q^2)}{3\hat{s}^2}\left(\frac{\hat{s}}{\hat{t}} + \frac{\hat{t}}{\hat{s}}\right), \quad (2.3)$$

For the LT contribution, we found

$$\Sigma_M^{LT} \equiv E \frac{d\sigma}{d^3p} = \sum_q \int_0^1 dx_1 dx_2 dz \left( G_{q_1/h_1}(x_1, Q_1^2) G_{q_2/h_2}(x_2, Q_2^2) D_g^\rho(z) \frac{\hat{s}}{\pi z^2} \frac{d\sigma}{d\hat{t}}(q\bar{q} \rightarrow g\gamma) + \right. \\ \left. G_{q_1/h_1}(x_1, Q_1^2) G_{g/h_2}(x_2, Q_2^2) D_q^\rho(z) \frac{\hat{s}}{\pi z^2} \frac{d\sigma}{d\hat{t}}(qg \rightarrow q\gamma) \right) \delta(\hat{s} + \hat{t} + \hat{u}), \quad (2.4)$$

where

$$\hat{s} = x_1 x_2 s, \quad \hat{t} = \frac{x_1 t}{z}, \quad \hat{u} = \frac{x_2 u}{z}, \quad z = -\frac{x_1 t + x_2 u}{x_1 x_2 s}. \quad (2.5)$$

$G_{q_{1,2}/h_{1,2}}(x, Q^2)$  and  $G_{g/h}(x, Q^2)$  are the quark(antiquark) and gluon distribution function inside a proton and antiproton, respectively.  $D_g^\rho(z) = D_g^{\rho_L}(z) = D_g^{\rho_{\bar{L}}}(z)$  and  $D_q^{\rho_L}(z)$  are the gluon and the quark fragmentation function. The  $\delta$  function may be expressed in terms of the parton kinematic variables, and the  $z$  integration may then be done. The final form for the cross section is obtained as

$$\Sigma_M^{LT} \equiv E \frac{d\sigma}{d^3p} = \sum_q \int_{x_{1min}}^{x_{1max}} dx_1 \int_{x_{2min}}^{x_{2max}} dx_2 \int_0^1 dz \left( G_{q_1/h_1}(x_1, Q_1^2) G_{q_2/h_2}(x_2, Q_2^2) \cdot \right. \\ \left. \cdot D_g^{\rho_L}(z) \frac{\hat{s}}{\pi z^2} \frac{d\sigma}{d\hat{t}}(q\bar{q} \rightarrow g\gamma) + G_{q_1/h_1}(x_1, Q_1^2) G_{g/h_2}(x_2, Q_2^2) D_q^{\rho_L}(z) \cdot \frac{\hat{s}}{\pi z^2} \frac{d\sigma}{d\hat{t}}(qg \rightarrow q\gamma) \right) = \\ = \sum_q \int_{x_{1min}}^{x_{1max}} dx_1 \int_{x_{2min}}^{x_{2max}} \frac{dx_2}{-(x_1 t + x_2 u)} \left( x_1 G_{q_1/h_1}(x_1, Q_1^2) s x_2 G_{q_2/h_2}(x_2, Q_2^2) \frac{D_g^{\rho_L}(z)}{\pi} \cdot \right. \\ \left. \cdot \frac{d\sigma}{d\hat{t}}(q\bar{q} \rightarrow g\gamma) + x_1 G_{q_1/h_1}(x_1, Q_1^2) s x_2 G_{g/h_2}(x_2, Q_2^2) \frac{D_q^{\rho_L}(z)}{\pi} \frac{d\sigma}{d\hat{t}}(qg \rightarrow q\gamma) \right), \quad (2.6)$$

where

$$x_{1min} = \frac{p_T e^y}{\sqrt{s} - p_T e^{-y}}, \quad x_{2min} = \frac{x_1 p_T e^{-y}}{x_1 \sqrt{s} - p_T e^y}.$$

In really in Eq.(2.6) the region of integration we took from  $x_{1min}$  to  $x_{1max}$ , and  $x_{2min}$  to  $x_{2max}$  which here  $x_1$  is changed in this interval  $x_1 \in [0.033 \div 0.925]$ , so  $x_{1min} = 0.033$ ,  $x_{1max} = 0.925$  and  $x_2$  is changed in this interval  $x_2 \in [0.001 \div 0.857]$ , so  $x_{2min} = 0.001$ ,  $x_{2max} = 0.857$ . Thus, here  $x_{1max}$  is not equal to unite, so  $(x_{1max} - 1) \neq 0$ . Therefore, here  $\alpha_s$  have not any infrared singularity

### III. HIGHER TWIST CONTRIBUTIONS TO INCLUSIVE DIRECT LONGITUDINALLY POLARIZED $\rho_L$ MESON PRODUCTION

The HT Feynman diagrams are shown in Fig.1. According to factorization theorem, the HT amplitude  $M$  can be factored in terms of the elementary hard-scattering amplitude ( $T_H$ ) and hadron DA ( $\Phi_{\rho_L}$ ) for directly produced  $\rho_L$  meson. We have aimed to calculate the  $\rho_L$  meson production cross-section and to fix the differences due to the use of various  $\rho_L$  meson DAs. The amplitude for this subprocess can be found by means of the Brodsky-Lepage formula [19]

$$M(\hat{s}, \hat{t}) = \int_0^1 dx_1 \int_0^1 dx_2 \delta(1 - x_1 - x_2) \Phi_M(x_1, x_2, Q^2) T_H(x_1, x_2; Q^2, \mu_R^2, \mu_F^2) \quad (3.1)$$

It is well know that, the hard-scattering amplitude  $T_H(x_1, x_2; Q^2, \mu_R^2, \mu_F^2)$  in Eq.(3.1) depends on a process and can be obtained in the framework of pQCD and represented as a series in the QCD running coupling constant  $\alpha_s(Q^2)$ . The light-cone momentum fractions  $x \equiv x_1$ ,  $x_2 = 1 - x$  specify the fractional momenta carried by quark and antiquark in the Fock state.

At the leading order of pQCD calculations, the hard scattering amplitude  $T_H(x_1, x_2; Q^2, \mu_R^2, \mu_F^2)$  does not depend on the factorization scale  $\mu_F^2$ , but strongly depends on renormalization scale  $\mu_R^2$ . However, the scales  $\mu_F^2$  and  $\mu_R^2$  are independent of each other. Therefore, it does not depend on the choice of the renormalization scale or the factorization scale.

Note that in our calculations for renormalization scale we use the momentum squared carried by the hard gluon (virtuality of gluon) which can be seen directly from Fig.1. Natural way, to obtain the expression for the momentum square is comes from the application of the

four-momentum conservation law to Fig.1. We eventually find the expression for  $Q_1^2(x)$  as:  $Q_1^2(x) = -(1 - x_1)\hat{u}$  while  $Q_2^2(x) = -x_1\hat{t}$ .

Thus, we have shown the reason of the choosing renormalization scale. The rest of the results we have presented in this paper are based on the above reasoning. Thus as noted in above, the choosing renormalization scale (virtuality of hard gluon) is not conjectural.

In calculations of  $T_H$ , we have neglected external lines and also rho meson mass. Furthermore, we considered the fact that initial quarks combine to form color neutral particles, which are restricted to be in the spin state of the final rho meson.

The cross-section for the HT subprocess is given by the expression

$$\frac{d\sigma}{d\hat{t}}(\hat{s}, \hat{t}, \hat{u}) = \frac{8\pi^2\alpha_E C_F}{27} \frac{[G(\hat{t}, \hat{u})]^2}{\hat{s}^3} \left[ \frac{1}{\hat{u}^2} + \frac{1}{\hat{t}^2} \right], \quad (3.2)$$

where

$$G(\hat{t}, \hat{u}) = e_1\hat{t} \int_{x_{1min}}^{x_{1max}} dx_1 \left[ \frac{\alpha_s(Q_1^2)\Phi_{\rho_L}(x_1, Q_1^2)}{1 - x_1} \right] + e_2\hat{u} \int_{x_{1min}}^{x_{1max}} dx_1 \left[ \frac{\alpha_s(Q_2^2)\Phi_{\rho_L}(x_1, Q_2^2)}{1 - x_1} \right], \quad (3.3)$$

where  $e_1(e_2)$  is the charge of  $q_1(\bar{q}_2)$  and  $C_F = \frac{4}{3}$ .

First, it seems that even the integral (3.3) has a singularity, since the  $\rho$  meson function ( $\Phi_\rho$ ) is the order of  $(1 - x)$  (see Eqs.(3.9 - 3.13)) it does not have any divergency problem. Another side in Eq.(3.3), in the region of integration, we adopt from  $x_{1min}$  to  $x_{1max}$ , in which here  $x_1$  is changed in this interval  $x_1 \in [0.033 \div 0.925]$ , also here  $x_{1max}$  is not equal to unite, so  $(x_{1max} - 1) \neq 0$ . According of the values  $x_{1,2}$ , the minimal value of  $Q_{1,2}^2$  accepts the value of (120.668, 4.237). Therefore, here,  $\alpha_s$  has not got any infrared singularity. The HT contribution to the large- $p_T$  longitudinally polarized  $\rho_L$  meson production cross-section in the process  $pp \rightarrow \rho_L^\pm \gamma X$  [5] is

$$\Sigma_M^{HT} \equiv E \frac{d\sigma}{d^3p} = \int_0^1 \int_0^1 dx_1 dx_2 G_{q_1/h_1}(x_1, Q_1^2) G_{q_2/h_2}(x_2, Q_2^2) \frac{\hat{s}}{\pi} \frac{d\sigma}{d\hat{t}}(q\bar{q} \rightarrow \rho_L \gamma) \delta(\hat{s} + \hat{t} + \hat{u}) = \frac{1}{\pi} \frac{d\sigma}{dy dp_T^2}. \quad (3.4)$$

The Mandelstam variables  $t$  and  $u$  also can be expressed in terms of the process center-of-mass energy, transverse momentum of  $\rho_L$  meson, and the rapidity by using the following expressions:

$$\begin{aligned} \hat{t} &= x_1 t, \\ \hat{u} &= x_2 u, \end{aligned} \quad (3.5)$$

$$t = -m_T \sqrt{s} e^{-y} = -p_T \sqrt{s} e^{-y},$$

$$u = -m_T \sqrt{s} e^y = -p_T \sqrt{s} e^y.$$

Using the relation in Eq.(3.5) and the fact that for the massless two-body scattering  $\hat{s} + \hat{t} + \hat{u} = 0$ , we obtain

$$x_1 = -\frac{x_2 u}{x_2 s + t} = \frac{x_2 p_T \sqrt{s} e^y}{x_2 s - p_T \sqrt{s} e^{-y}},$$

$$x_2 = -\frac{x_1 t}{x_1 s + u} = \frac{x_1 p_T \sqrt{s} e^{-y}}{x_1 s - p_T \sqrt{s} e^y},$$

where  $m_T$  is the transverse mass of  $\rho_L$  meson, which is given by

$$m_T^2 = m^2 + p_T^2.$$

For a full discussion and for the possible extraction of the HT contributions to cross-section, we calculated difference of the cross-sections of the longitudinally polarized  $\rho_L$  meson production in proton-antiproton and proton-proton collisions. It should be noted that a similar approach is widely applied in the extraction of the contribution of the spin effects to the one and double spin asymmetries:

$$\Delta = \Sigma_{p\bar{p}} - \Sigma_{pp} \quad (3.6)$$

where,

$$\Sigma_{p\bar{p}} = E_{\rho_L^+} \frac{d^3\sigma}{d^3p} (p\bar{p} \rightarrow \rho_L^+ + \gamma + X) + E_{\rho_L^-} \frac{d^3\sigma}{d^3p} (p\bar{p} \rightarrow \rho_L^- + \gamma + X) \quad (3.7)$$

and

$$\Sigma_{pp} = E_{\rho_L^+} \frac{d^3\sigma}{d^3p} (pp \rightarrow \rho_L^+ + \gamma + X) + E_{\rho_L^-} \frac{d^3\sigma}{d^3p} (pp \rightarrow \rho_L^- + \gamma + X)$$

In this study, we utilized the following  $\rho_L$  meson DAs: asymptotic DAs  $\Phi_{\rho_L}^{asy}(x)$ , derived in pQCD evaluation, Ball-Braun  $\Phi_{\rho_L}^{BB}(x, Q^2)$  DA obtained by using QCD sum rules [20],  $\Phi_{\rho_L}^{PMS}(x, Q^2)$  is obtained by Pimikov *et al.* [21] by using QCD sum rules,  $\Phi_{\rho_L}^{Linear}(x, Q^2)$ , and  $\Phi_{\rho_L}^{HO}(x, Q^2)$  DAs obtained by Choi and Ji [22] from linear and harmonic oscillator potential model, respectively.



The principle definition of DA of the  $\rho$  meson have the form [20]:

$$\begin{aligned} \langle 0 | \bar{u}(0)\gamma_\mu d(x) | \rho^+(p, \lambda) \rangle = & p_\mu \frac{(e^{(\lambda)}x)}{(px)} f_\rho m_\rho \int_0^1 du e^{-iupx} \Phi_{\rho_L}(u, \mu) \\ & (e_\mu^{(\lambda)} - p_\mu \frac{(e^{(\lambda)}x)}{(px)}) f_\rho m_\rho \int_0^1 du e^{-iupx} g_\perp^{(v)}(u, \mu) \end{aligned} \quad (3.8)$$

Should be noted that for construction DA for the light mesons  $\Phi_\rho(x, \mu_0^2)$  is taken massless and normalized to unit. They are defined by the following expressions:

$$\Phi_{\rho_L}^{asy}(x) = 6x(1-x) \quad (3.9)$$

$$\Phi_{\rho_L}^{BB}(x, \mu_0^2) = \Phi_{\rho_L}^{asy}(x) \left[ C_0^{3/2}(2x-1) + 0.18 \cdot C_2^{3/2}(2x-1) \right], \quad (3.10)$$

$$\begin{aligned} \Phi_{\rho_L}^{PMS}(x, \mu_0^2) = \Phi_{\rho_L}^{asy}(x) \left[ C_0^{3/2}(2x-1) + 0.047 \cdot C_2^{3/2}(2x-1) - \right. \\ \left. - 0.057 \cdot C_4^{3/2}(2x-1) \right], \end{aligned} \quad (3.11)$$

$$\begin{aligned} \Phi_{\rho_L}^{Linear}(x, \mu_0^2) = \Phi_{\rho_L}^{asy}(x) \left[ C_0^{3/2}(2x-1) + 0.02 \cdot C_2^{3/2}(2x-1) - 0.01 \cdot C_4^{3/2}(2x-1) - \right. \\ \left. 0.02 \cdot C_6^{3/2}(2x-1) \right], \end{aligned} \quad (3.12)$$

$$\begin{aligned} \Phi_{\rho_L}^{HO}(x, \mu_0^2) = \Phi_{\rho_L}^{asy}(x) \left[ C_0^{3/2}(2x-1) - 0.02 \cdot C_2^{3/2}(2x-1) - 0.03 \cdot C_4^{3/2}(2x-1) - \right. \\ \left. 0.02 \cdot C_6^{3/2}(2x-1) \right], \end{aligned} \quad (3.13)$$

where  $C_n^{3/2}(2x-1)$  are Gegenbauer polynomials. In the numerical calculations for normalization scale  $\mu_0^2$  we adopt  $\mu_0^2 = 1\text{GeV}^2$ . Also, non-trivial Gegenbauer moments  $a_n$  have been taken at the scale  $\mu_0^2 = 1\text{GeV}^2$ .

The DAs of mesons, specially of  $\pi$  and  $\rho$  meson also are developed in Refs. [23–28] by the Dubna group. Some properties of Gegenbauer polynomials given in App. A

#### IV. NUMERICAL RESULTS AND DISCUSSION

In this section, we discuss in detail the numerical predictions of the LT and HT cross-sections of the direct  $\rho_L$  meson production processes  $pp \rightarrow \rho_L \gamma X$  and  $p\bar{p} \rightarrow \rho_L \gamma X$  at

the 62.4 GeV energies taking into account the full leading-order contributions from quark-antiquark annihilation process. For the HT subprocess, we take  $q_1 + \bar{q}_2 \rightarrow (q_1 \bar{q}_2) + \gamma$  and for the dominant LT subprocess for the  $\rho_L$  meson production, we take the quark-antiquark annihilation  $q\bar{q} \rightarrow g\gamma$ , in which the  $\rho_L^\pm$  meson is indirectly emitted from the gluon and quark-gluon fusion,  $qg \rightarrow q\gamma$ , with subsequent fragmentation of final quark into a meson,  $q \rightarrow \rho_L^\pm$ . We denote the HT cross-section by  $\Sigma_\rho^{HT}$ , the LT cross-section by  $\Sigma_\rho^{LT}$ . For the quark and gluon distribution functions inside the proton and antiproton, the MSTW2008 PDFs [29] and the quark and gluon fragmentation functions [30] are used. Also, the following abbreviations are defined for DAs: asy is  $\Phi_{\rho_L}^{asy}(x)$ , BB is  $\Phi_{\rho_L}^{BB}(x, Q^2)$ , PMS is  $\Phi_{\rho_L}^{PMS}(x, Q^2)$ , Linear is  $\Phi_{\rho_L}^{Linear}(x, Q^2)$ , and HO is  $\Phi_{\rho_L}^{HO}(x, Q^2)$ . The results are given for  $\sqrt{s} = 62.4$  GeV on the transverse momentum  $p_T$  ranging from 2 GeV/ $c$  to 30 GeV/ $c$  which are also valid for the PHENIX experiment. Obtained results are visualized through Figs. 2-11.

First of all, it is very interesting to compare the HT cross-sections for all DAs of the  $\rho$  meson. In Figs. 2- 8, we show the HT cross-section  $\Sigma_{\rho_L^\pm}^{HT}$  and  $\Sigma_{\rho_L^\pm}^{HT}$  of the process  $p\bar{p} \rightarrow \rho_L^\pm \gamma X$ , the difference of the cross-sections  $\Delta = \Sigma_{p\bar{p}} - \Sigma_{pp}$  and the ratio  $\Sigma_\rho^{HT}/\Sigma_\rho^{LT}$ , and  $\Delta/\Sigma_\rho^{LT}$  as a function of the meson transverse momentum  $p_T$  for the DAs which is presented by Eqs. (3.9) - (3.13) and for  $y = 0$ .

As is seen from Figs. 2- 5 the HT  $\Sigma_{\rho_L^\pm}^{HT}$  and  $\Sigma_{\rho_L^\pm}^{HT}$  cross-sections are monotonically decreasing with an increase in the transverse momentum of the  $\rho_L$  meson. It is worth to mention that at the c.m. energy  $\sqrt{s}=62.4$  GeV the maximum value of the cross-section of the process  $p\bar{p} \rightarrow \rho_L^\pm \gamma X$  for the  $\Phi_{\rho_L}^{BB}(x, Q^2)$  decreases from the interval  $1.7 \times 10^{-4}$  mb/GeV<sup>2</sup> to  $5.352 \times 10^{-20}$  mb/GeV<sup>2</sup>, but the maximum value of the cross-section of the process  $pp \rightarrow \rho_L^\pm \gamma X$  for the  $\Phi_{\rho_L}^{BB}(x, Q^2)$  decreases from the interval  $1.992 \times 10^{-4}$  mb/GeV<sup>2</sup> to  $2.634 \times 10^{-24}$  mb/GeV<sup>2</sup>. The magnitude for the difference of the cross-sections  $\Delta$  for  $\Phi_{\rho_L}^{BB}(x, Q^2)$  decreases from the interval  $9.757 \times 10^{-6}$  mb/GeV<sup>2</sup> to  $5.566 \times 10^{-20}$  mb/GeV<sup>2</sup>. It can be seen that the difference of cross-sections  $\Delta$  is slowly decreasing with an increase in the transverse momentum of the  $\rho_L$  meson.

Through Figs. 7 and 8, we have displayed the ratio  $\Sigma_\rho^{HT}/\Sigma_\rho^{LT}$ , and  $\Delta/\Sigma_\rho^{LT}$  as a function of the meson transverse momentum  $p_T$  for the DAs which is presented by Eqs. (3.9) - (3.13) and for  $y = 0$ . The ratio for all DAs has a minimum at approximately  $p_T = 15$  GeV/ $c$  and after this, the value increases monotonically with an increase in the transverse momentum of the  $\rho_L$  meson. Ratio of  $\Sigma_{p\bar{p}}^{HT}/\Sigma_\rho^{LT}$  for  $\Phi_{\rho_L}^{BB}(x, Q^2)$  DA is changed the interval between

$1.40839 \times 10^4$  to  $1.2903 \times 10^6$ , for  $\Phi_{\rho_L}^{Linear}(x, Q^2)$  DA is changed in the interval between  $7.8656 \times 10^3$  to  $8.2459 \times 10^5$ . However, for ratio  $\Delta/\Sigma_{\rho}^{LT}$  for  $\Phi_{\rho_L}^{BB}(x, Q^2)$  DA is changed in the interval between  $3.6494 \times 10^2$  to  $1.2903 \times 10^6$ , for  $\Phi_{\rho_L}^{Linear}(x, Q^2)$ , DA is changed in the interval between  $1.937 \times 10^2$  to  $8.245 \times 10^5$ . As is seen from Fig.7 and 8, the ratio of HT to LT cross sections for the dependence on the  $p_T$  has a similar behavior.

Finally in Figs. 9-11, we have presented the HT cross-sections  $\Sigma_{p\bar{p}}^{HT}$ ,  $\Sigma_{pp}^{HT}$  and difference  $\Delta = \Sigma_{p\bar{p}} - \Sigma_{pp}$  as a function of the rapidity  $y$  of the  $\rho_L$  meson at c.m.energy 62.4 GeV and  $p_T=4.9$  GeV/ $c$ . At 62.4 GeV and  $p_T=4.9$  GeV/ $c$ , the meson rapidity lies in the region  $-2.52 \leq y \leq 2.52$ . As is seen from figures, the cross-sections and difference of cross-sections for all DAs increase with an increase of the  $y$  rapidity of the meson and have a maximum approximately at the point  $y = 1.5$ . After reaching the maximum, it is decreasing rapidly with an increase in the transverse momentum of the  $\rho_L$  meson. As it is seen from Fig. 10 in the region  $(-2.52 \leq y \leq 0.96)$ , the ratio for all DAs increase and it has a maximum approximately at the point  $y = 0.96$ . Similarly, the ratio decreases with an increase in the  $y$  rapidity of the  $\rho_L$  meson. It can also be seen that the ratios are sensitive to the choice of the meson DAs. In Fig.11 we present difference  $\Delta = \Sigma_{p\bar{p}} - \Sigma_{pp}$  as a function of the rapidity  $y$  of the  $\rho_L$  meson.

For the HT contribution, it is important to analyze its relative magnitude of contribution compared to the LT contribution, since only LT diagrams are commonly considered in usual studies of the hadron-hadron collision. As seen from the figures, HT contributions are comparable with the cross-section of LT in the region  $p_T < 10$  GeV/ $c$ . Moreover, in the region  $p_T < 5$  GeV/ $c$  HT contributions become more significant.

Thus, it can be concluded that HT cross-section of the  $\rho_L$  meson production in the proton-antiproton and proton-proton collisions appears in the range and should be observable at the PHENIX and PANDA experiments.

## V. CONCLUSION

We have calculated and analyzed the cross-section of the direct inclusive longitudinally polarized  $\rho_L$  meson production via HT mechanism in the proton-proton and proton-antiproton collisions. We discussed the phenomenological consequences of possible HT contributions to cross-sections and also compared with LT. Moreover, in order to extract HT subprocesses

from LT background, we adopted different  $\rho_L$  meson DAs. In the numerical calculations, dependencies of the HT contribution on the transverse momentum and the rapidity of the  $\rho_L$  meson are discussed with special emphasis on DAs. Analysis of our results show that with increasing  $p_T$ , the HT contributions decrease more rapidly than LT contributions. The preceding results demonstrate that HT contributions must be considered especially in the region of low  $p_T$ . It is shown that the HT contribution to the cross-section depends on the choice of the meson distributions amplitudes. Thus, it is crucial to note that the contribution of HT effects to cross-section the dependence on the DAs is weak. Despite that, the HT cross-section obtained in our study should be observable at hadron collider. Also, the feature of HT effects may help theoretical interpretations of the future experimental data for the direct inclusive vector meson production cross-section in the proton-proton and proton-antiproton collisions.

It is important to note that the difference of the cross-section  $\Delta = \Sigma_{p\bar{p}} - \Sigma_{pp}$  is not equal to zero. This enables to calculate and extract the extension of the HT to cross-section. It is also one of the most critical points for the experiment.

It can be noted that the HT processes for large- $p_T$  meson production have a key enabling contribution, where the  $\rho_L$  meson are generated directly in the hard-scattering subprocess, rather than by gluon and quark fragmentation. Inclusive  $\rho_L$  meson production provides an essential test case where HT contributions dominate those of LT in the certain kinematic regions. The HT contributions can be utilized to interpret theoretically the future experimental data for the charged  $\rho_L$  meson production in  $pp$  and  $p\bar{p}$  collisions. The results of this study can be useful to provide a simple test of the short distance structure of QCD as well as to determine more precise DAs of the  $\rho_L$  meson.

By taking these points into account, it may be argued that the analysis of the HT effects on the dependence of the  $\rho_L$  meson DAs in longitudinally polarized  $\rho_L$  meson production at proton-proton and proton-antiproton collisions is significant in both theoretical and experimental studies.

## Appendix A: Gegenbauer polynomials and its some properties

The  $\rho_L$  meson DA is symmetric under replacement  $x_1 - x_2 \leftrightarrow x_2 - x_1$ . Thus,  $x \equiv x_1$ ,  $x_2 = 1 - x$  and  $x_1 - x_2 = 2x - 1$ . A recurrence relation for Gegenbauer polynomials is:

$$nC_n^{(\lambda)}(\xi) = 2(n + \lambda - 1)\xi C_{n-1}^{(\lambda)}(\xi) - (n + 2\lambda - 2)C_{n-2}^{(\lambda)}(\xi). \quad (\text{A1})$$

Also, the few Gegenbauer polynomials in expression (3.9) - (3.13) are as follows:

$$\begin{aligned} C_0^{3/2}(2x - 1) &= 1, \quad C_2^{3/2}(2x - 1) = \frac{3}{2}(5(2x - 1)^2 - 1), \\ C_4^{3/2}(2x - 1) &= \frac{15}{8}(21(2x - 1)^4 - 14(2x - 1)^2 + 1), \\ C_6^{3/2}(2x - 1) &= \frac{1}{16}(3003(2x - 1)^6 - 3465(2x - 1)^4 + 945(2x - 1)^2 - 35). \end{aligned} \quad (\text{A2})$$

The  $\rho$  meson DA can be expanded over the eigenfunctions of the one-loop Efremov-Radyushkin-Brodsky-Lepage (ERBL) equation [31–33]

$$\Phi_\rho(x, Q^2) = \Phi_{asy}(x) \left[ 1 + \sum_{n=2,4,\dots}^{\infty} a_n(Q^2) C_n^{3/2}(2x - 1) \right]. \quad (\text{A3})$$

The evolution of the DA on the factorization scale  $Q^2$  is handled by the functions  $a_n(Q^2)$  as

$$a_n(Q^2) = a_n^\parallel(\mu_0^2) \left[ \frac{\alpha_s(Q^2)}{\alpha_s(\mu_0^2)} \right]^{\gamma_n^\parallel/2\beta_0}, \quad (\text{A4})$$

Here, the strong coupling constant  $\alpha_s(Q^2)$  at the one-loop approximation is given as

$$\alpha_s(Q^2) = \frac{4\pi}{\beta_0 \ln(\frac{Q^2}{\Lambda^2})}. \quad (\text{A5})$$

where  $\Lambda$  is the QCD scale parameter,  $\beta_0$  is the QCD beta function one-loop coefficients defined as

$$\beta_0 = 11 - \frac{2}{3}n_f.$$

In expression (A4)  $\gamma_n$ 's are anomalous dimensions defined by the expression

$$\gamma_n^\parallel = \frac{8}{3} \left[ 1 - \frac{2}{(n+1)(n+2)} + 4 \sum_{j=2}^{n+1} \frac{1}{j} \right]. \quad (\text{A6})$$

So, from expression (A6) we obtain

$$\frac{\gamma_2^\parallel}{2\beta_0} = \frac{50}{81}, \quad \frac{\gamma_4^\parallel}{2\beta_0} = \frac{364}{405}, \quad \frac{\gamma_6^\parallel}{2\beta_0} = \frac{1027}{105} \quad (\text{A7})$$

The Gegenbauer moments  $a_n$  can be determined by using the Gegenbauer polynomials orthogonality condition

$$\int_{-1}^1 (1 - \xi^2) C_n^{3/2}(\xi) C_{n'}^{3/2}(\xi) d\xi = \frac{\Gamma(n+3) \delta_{nn'}}{n!(n+3/2)}. \quad (\text{A8})$$

The Gegenbauer moments  $a_n$  are very practical in studying the DAs because they form the shape of the corresponding hadron wave function. They can be derived from theoretical models or extracted from the experimental data. Besides, these moments reveal how much the DAs deviate from the asymptotic one.

### Acknowledgments

We cordially thank S. V. Mikhailov and A. V. Pimikov for many helpful and insightful discussions.

- 
- [1] J. C. Collins, D. E Soper, G.F.Sterman, *Adv. Ser. Dir. High Energy Phys.* **5**, 1 (1988).
  - [2] S. M. Berman, J. D. Bjorken, J. B. Kogut, *Phys. Rev. D.* **4**, 3388 (1971).
  - [3] E. L. Berger , *Phys. Rev. D.* **26**, 105 (1982).
  - [4] S. J. Brodsky, G. R. Farrar , *Phys. Rev. Lett.* **31**, 1153 (1973).
  - [5] J. F. Owens, *Rev. Mod. Phys.* **59**, 465 (1987).
  - [6] F. Arleo, *Nucl. Phys. B, Proc. Suppl.* **207** (2010).
  - [7] S. J. Brodsky, A. Sickles , *Phys. Lett. B.* **668**, 111 (2008).
  - [8] P. Ball, V. M. Braun , *Nucl. Phys. B* **543**, 201 (1999).
  - [9] S. J. Brodsky, G. L. Lepage, and P. B. Mackenzie, *Phys. Rev. D* **28**, 228 (1983).
  - [10] M. Mojaza, S. J. Brodsky and X. G.Wu, *Phys. Rev. Lett.* **110**, 192001 (2013).
  - [11] ALICE Collab. (E. Incani.), *Nucl. Phys. A.* **1** (2012).
  - [12] PANDA Collab.(W.Erni *et al*), arXiv:hep-ex/0903.3905.
  - [13] A. V. Luchinsky and S. V. Poslavsky, *Phys. Rev. D* **85**, 074016 (2012).
  - [14] A. I. Ahmadov, C. Aydin, and O. Uzun, *Phys. Rev. D.* **89**, 014018 (2014).
  - [15] A. I. Ahmadov, C. Aydin, and O. Uzun, *Phys. Rev. D.* **87**, 014006 (2013).
  - [16] A. I. Ahmadov, C. Aydin, F. Keskin, *Ann. Phys.* **327**, 1472 (2012).
  - [17] A. I. Ahmadov, C. Aydin, F. Keskin, *Phys. Rev. D.* **85**, 034009 (2012).

- [18] D. Du, T. Han, F. Kong, M. Luo, *Phys. Rev. D.* **36**, 745 (1987).
- [19] G. L. Lepage and S. J. Brodsky, *Phys. Rev. D* **22**, 2157 (1980).
- [20] P. Ball, V. M. Braun, *Phys. Rev. D.* **54**, 2182, (1996)
- [21] A. V. Pimikov, S. V. Mikhailov, N. G. Stefanis, *Few-Body Syst.* **55**, 401, (2014)
- [22] H. M. Choi and C. R. Ji, *Phys. Rev. D* **95**, 056002 (2017).
- [23] A. P. Bakulev, S. V. Mikhailov, and N. G. Stefanis, *Phys. Lett. B* **578**, 91 (2004).
- [24] A. P. Bakulev, S. V. Mikhailov, A. V. Pimikov, and N. G. Stefanis, *Phys. Rev. D* **86**, **031501** (2012).
- [25] A. P. Bakulev and S. V. Mikhailov, *Z. Phys. C* **68**, 451 (1995).
- [26] S. V. Mikhailov and A. V. Radyushkin, *Phys. Rev. D* **45**, 1754 (1992).
- [27] A. E. Dorokhov, *JETP Lett.* **77**, 63 (2003).
- [28] N. G. Stefanis and A. V. Pimikov. *Nucl. Phys.* **A945**, 248 (2016).
- [29] A. D. Martin, W. J. Stirling, R. S. Thorne, G. Watt, *Eur. Phys. J. C* **63**, 189 (2009).
- [30] H. Saveetha, D. Indumathi and S. Mitra, *Int. J. Mod. Phys. A* **27**, 1250103 (2012).
- [31] G. P. Lepage, S. J. Brodsky, *Phys. Lett.* **87** B, 359 (1979).
- [32] A. V. Efremov, A. V. Radyushkin, *Theor. Math. Phys.* **42**, 97 (1980).
- [33] A. V. Efremov, A. V. Radyushkin, *Phys. Lett.* **94** B, 245 (1980).

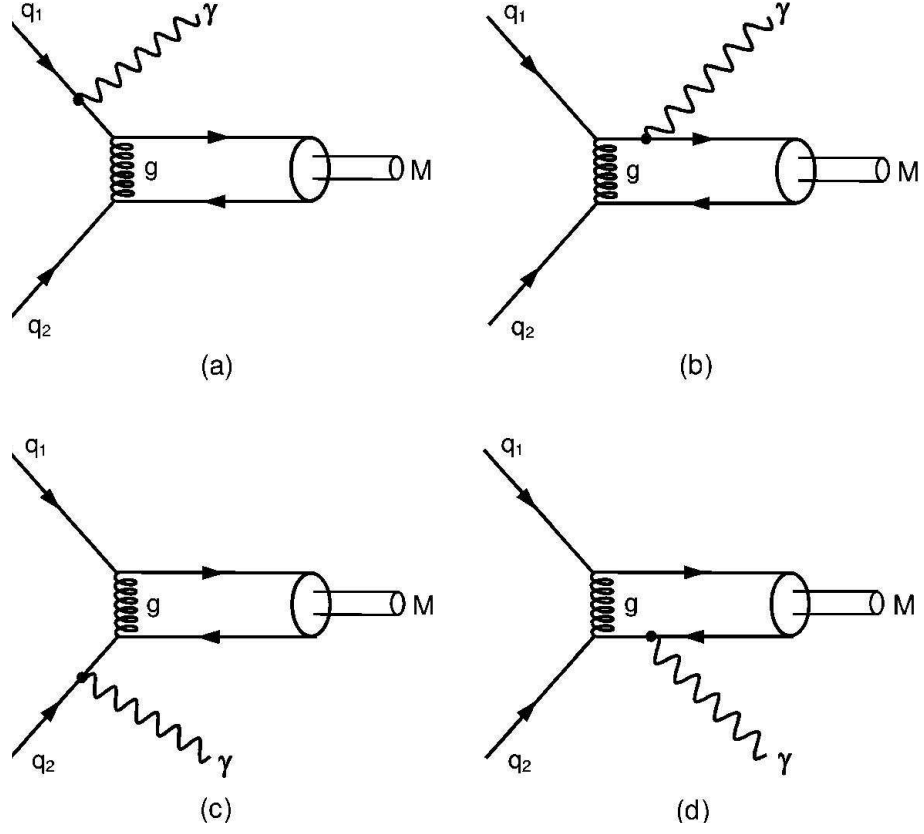


FIG. 1: Feynman diagrams for the HT subprocess,  $q_1 q_2 \rightarrow \rho_L^+ (or \rho_L^-) \gamma$ .



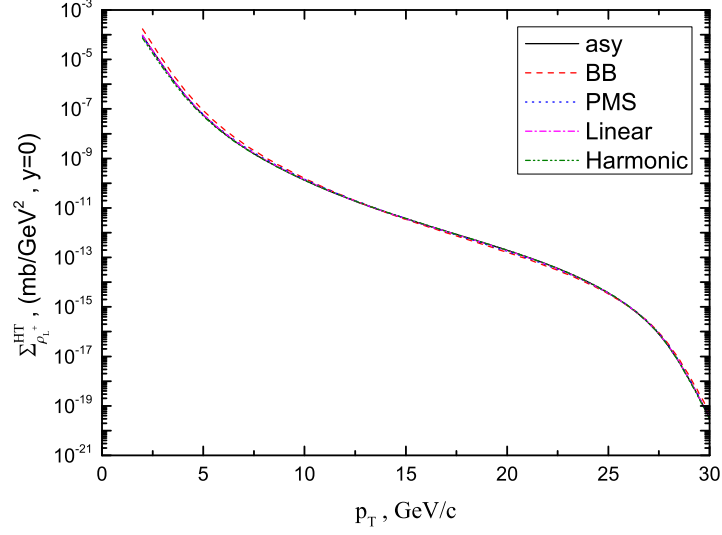


FIG. 2: HT contribution to  $\rho_L^+$  meson production  $p\bar{p} \rightarrow \rho_L^+ \gamma X$  cross-section  $\Sigma_{\rho^+}^{HT}$  as a function of the transverse momentum  $p_T$  of the  $\rho_L^+$  meson, at  $\sqrt{s} = 62.4$  GeV and  $y = 0$

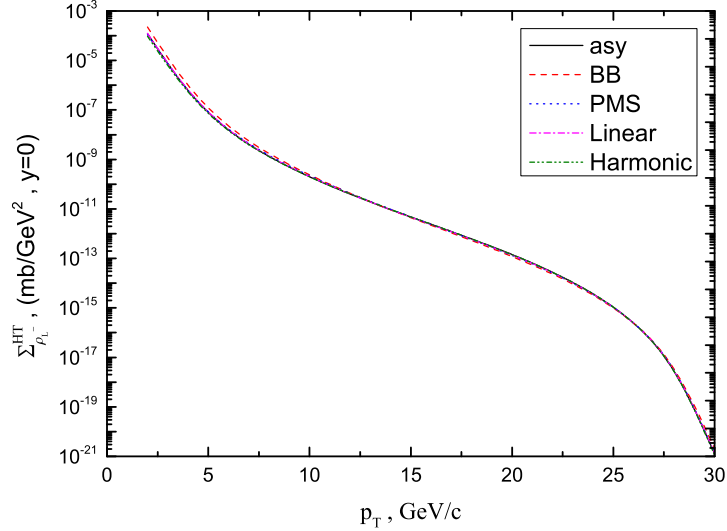


FIG. 3: HT contribution to  $\rho_L^-$  meson production  $p\bar{p} \rightarrow \rho_L^- \gamma X$  cross-section  $\Sigma_{\rho^-}^{HT}$  as a function of the transverse momentum  $p_T$  of the  $\rho_L^-$  meson, at  $\sqrt{s} = 62.4$  GeV and  $y = 0$

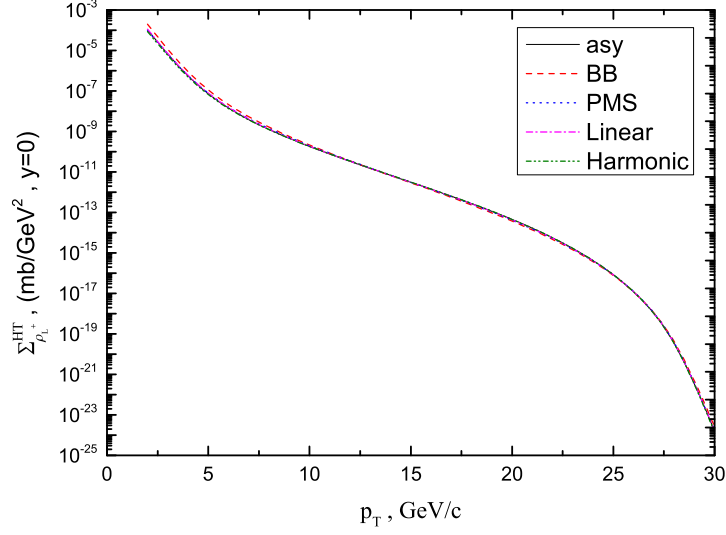


FIG. 4: HT contribution to  $\rho_L^+$  meson production  $pp \rightarrow \rho_L^+ \gamma X$  cross-section  $\Sigma_{\rho^+}^{HT}$  as a function of the transverse momentum  $p_T$  of the  $\rho_L^+$  meson, at  $\sqrt{s} = 62.4$  GeV and  $y = 0$

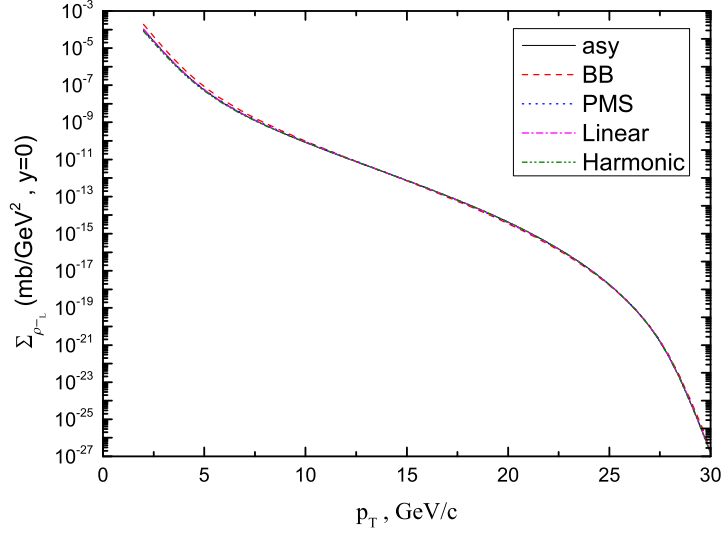


FIG. 5: HT contribution to  $\rho_L^-$  meson production  $pp \rightarrow \rho_L^- \gamma X$  cross-section  $\Sigma_{\rho^-}^{HT}$  as a function of the transverse momentum  $p_T$  of the  $\rho_L^-$  meson, at  $\sqrt{s} = 62.4$  GeV and  $y = 0$

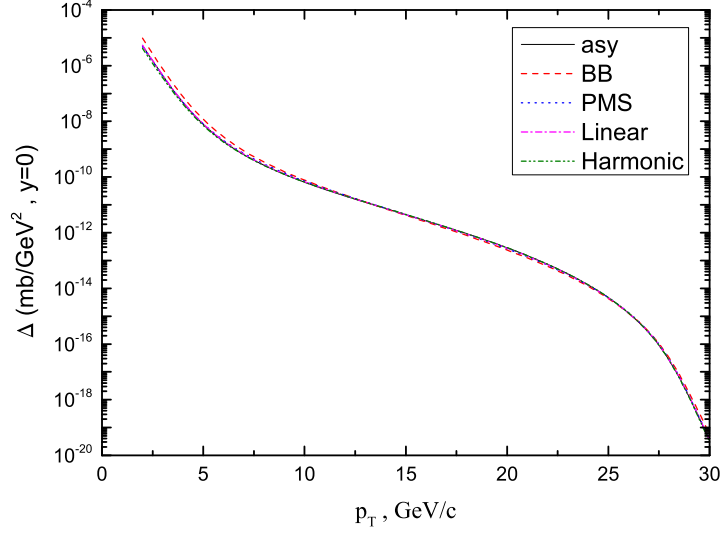


FIG. 6: HT contribution to difference of cross-section  $\Delta = \sum_{p\bar{p}} - \sum_{pp}$  as a function of the transverse momentum  $p_T$  of the  $\rho_L^+$  meson, at  $\sqrt{s} = 62.4$  GeV and  $y = 0$

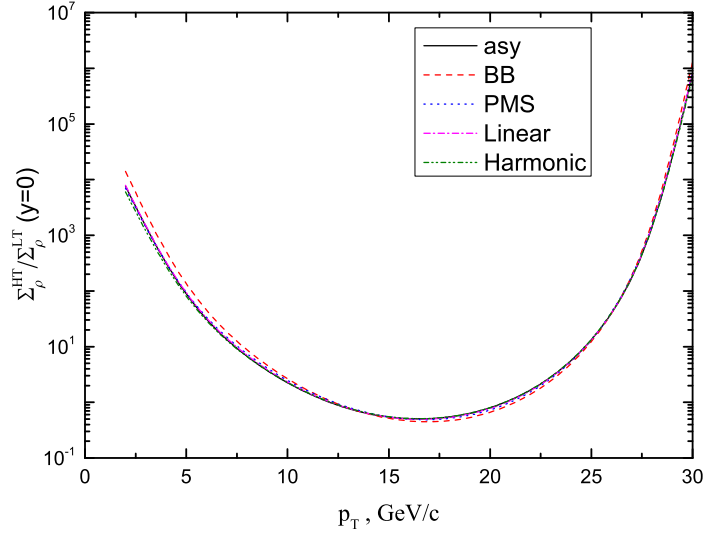


FIG. 7: Ratio  $\Sigma_{p\bar{p}}/\Sigma_{\rho}^{LT}$  as a function of the transverse momentum  $p_T$  of the  $\rho$  meson at the c.m. energy  $\sqrt{s}=62.4$  GeV and  $y = 0$ .

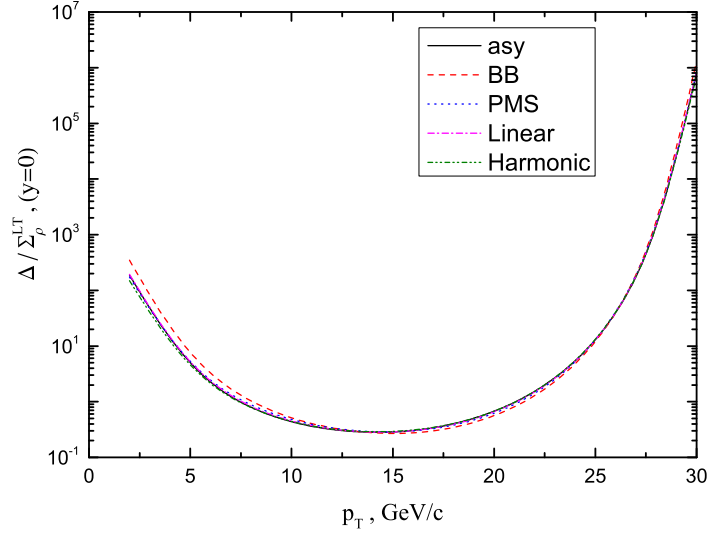


FIG. 8: Ratio  $\Delta/\Sigma_\rho^{LT}$  as a function of the transverse momentum  $p_T$  of the  $\rho$  meson at the c.m. energy  $\sqrt{s}=62.4$  GeV and  $y = 0$ .

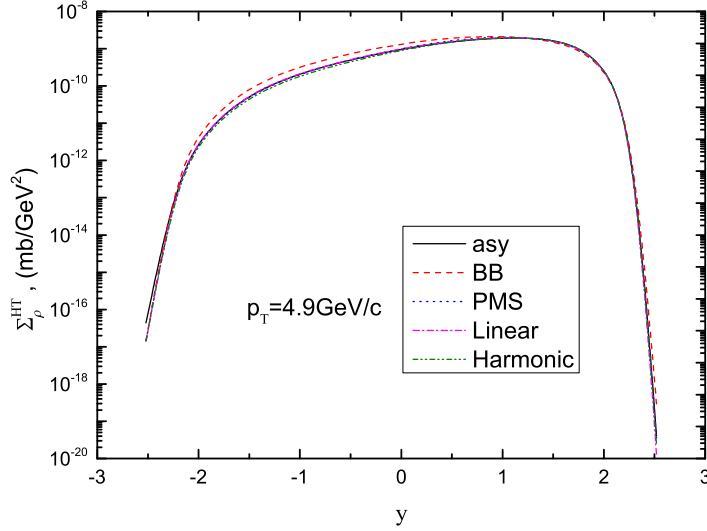


FIG. 9: HT contribution to sum of  $\rho_L$  meson production  $p\bar{p} \rightarrow \rho_L \gamma X$  cross-section  $\Sigma_{p\bar{p}}$  as a function of the  $y$  rapidity of the meson at  $p_T=4.9$  GeV/c, at  $\sqrt{s} = 62.4$  GeV.

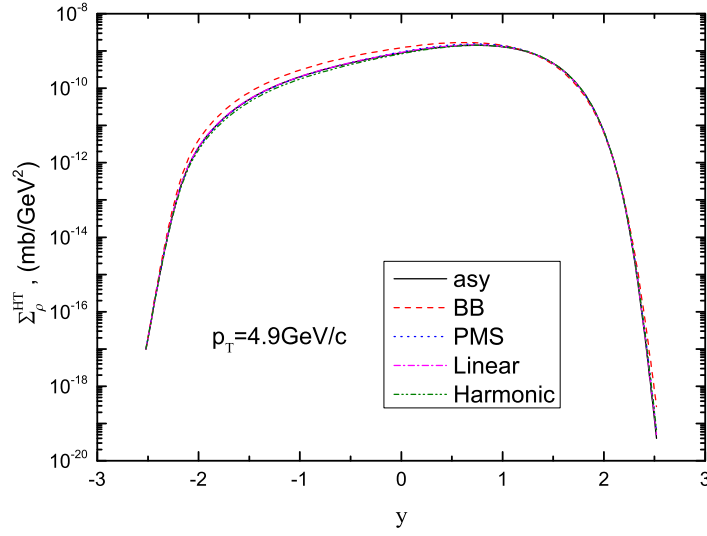


FIG. 10: HT contribution to sum of  $\rho_L$  meson production  $pp \rightarrow \rho_L \gamma X$  cross-section  $\Sigma_{pp}$  as a function of the  $y$  rapidity of the meson at  $p_T=4.9$  GeV/ $c$ , at  $\sqrt{s}=62.4$  GeV.

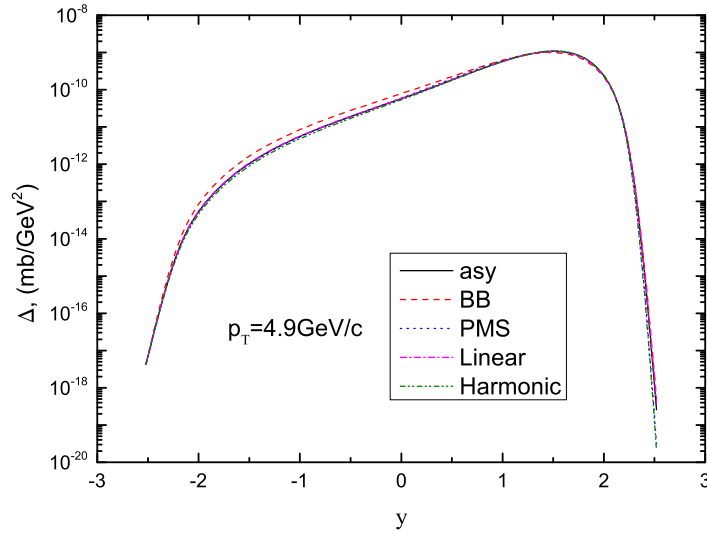


FIG. 11: HT contribution to difference of cross-section  $\Delta = \Sigma_{p\bar{p}} - \Sigma_{pp}$  as a function of the  $y$  rapidity of the meson at  $p_T=4.9$  GeV/ $c$ , at  $\sqrt{s}=62.4$  GeV.